Dielectric Separation of Minerals

By C. E. Jordan and G. V. Sullivan

As the Nation's principal conservation agency, the Department of the Interior has responsibility for most of our nationally owned public lands and natural resources. This includes fostering the wisest use of our land and water resources, protecting our fish and wildlife, preserving the environment and cultural values of our national parks and historical places, and providing for the enjoyment of life through outdoor recreation. The Department assesses our energy and mineral resources and works to assure that their development is in the best interests of all our people. The Department also has a major responsibility for American Indian reservation communities and for people who live in island territories under U.S. administration.

CONTENTS

ILLUSTRATIONS

TABLES

UNIT OF MEASURE ABBREVIATIONS USED IN THIS REPORT

C	coulomb	m^2	square meter
cm	centimeter	mdyn	millidyne
°C	degree Celsius	mho·m	mho meter
cm^3/cm	cubic centimeter per centimeter	mho/cm	mho per centimeter
cm/s^2	centimeter per square second	min	minute
cP	centipoise	mm	millimeter
dyn	dyne	P	poise
erg/°	erg per degree	pct	percent
g	gram	pF	picofarad
g/cm^3	gram per cubic centimeter	pF/cm	picofarad per centimeter
g/m^2	gram per meter squared	r/min	revolution per minute
g/min	gram per minute	s	second
h	hour	V	volt
Hz	hertz	W	watt
kHz	kilohertz	W/cm	watt per centimeter
(kW·h)/mt	kilowatt hour per metric ton	wt pct	weight percent
m	meter	μm	micrometer

SYMBOLS USED IN THIS REPORT

a	particle radius	q	charge
A_f	dielectric force area	R	radius of drum electrode
B	Boltzmann constant	r	radial distance
C	capacitance	r_w	wire radius
$\cos \phi$	power factor	s	distance
D	drum rotation speed	S_E	electrode spacing
E	electric field	S_f	fluid velocity
∇E	electric field gradient	S_{m_i}	distance between a wire and imaginery wire
F	force		
F_d	diffusion force	S_p	particle velocity
F_e	dielectric force	S_w	distance between drum-electrode wires
F_g	gravitational force		
F_i	inertial or centrifugal force	T	absolute temperature
F_j	current-induced polarization force	t	time
F_μ	viscous drag or fluid drag force	$\tan \delta$	tangent loss factor
G	conductance	V	voltage
g	acceleration of gravity	Z	impedance
i	imaginary unit vector	δ_i	angle from drum-electrode wire to particle location
K	dielectric constant		
L_w	length of drum-electrode wires	ϵ	electrical permittivity
N	concentration of particles	$\hat{\epsilon}$	complex permittivity
n	number of drum-electrodes wires opposing screen electrode	ϵ_0	permittivity of free space
		Θ	rotation angle of drum electrode
N_w	number of wires per revolution	Λ	linear charge density
P	power	μ	viscosity
p	moment	ϱ	density
		σ	electrical conductivity
		ω	angular frequency

DIELECTRIC SEPARATION OF MINERALS

By C. E. Jordan[1] and G. V. Sullivan[2]

ABSTRACT

The fundamental properties of dielectric separation were studied to provide insight into the design and operating characteristics of a dielectric separator. Force equations on mineral particles were derived and evaluated experimentally. Responses to variations in the electrical voltage and frequency, feed rate, particle size, dielectric fluid, and dielectric constant were tested theoretically and experimentally, using a 5-cm-diam dielectric separator.

High-dielectric mineral recovery was proportional to the calculated effective dielectric force volume (EDFV) that surrounded each drum-electrode wire. Electrode spacing was the most sensitive design parameter; spacing of less than 0.4 cm was required for a good separation. Dielectric separation was effective for separating minerals with dielectric constants that differed by approximately 2 or more.

[1]Supervisory metallurgist.
[2]Research supervisor.
Tuscaloosa Research Center, Bureau of Mines, Tuscaloosa, AL.

INTRODUCTION

Only a very small percentage of the ore taken from a mine contains the mineral values to be recovered. If these mineral values are present as distinct phases, they may be physically separated from the waste rock to reduce the quantity of material that must be subsequently processed. Physical separation is accomplished by utilizing differences in physical or surface chemical properties of the minerals to be separated. Magnetic, electrostatic, and gravity separation are well-known examples of separation methods based on differences in magnetic susceptibility, electrical conductivity, and density, respectively. Froth flotation utilizes differences in surface chemistry to enable separation. This report examines the use of differences in dielectric properties to achieve mineral separation.

All separation processes are based on an ability to selectively exert forces on the mineral particles to be recovered, causing them to move in a different direction from that of the particles to be discarded. For example, a magnetic mineral will be attracted to a magnet, or a negatively charged mineral will be attracted to a positively charged electrode. These and other separation methods can be used to selectively recover mineral values by separating them from the gangue minerals. Recovery by separation depends on differences in magnitude of the physical properties of the materials to be separated. Thus, two magnetic materials can be separated if one has a larger magnetic susceptibility than the other. Similarly, separations can be made based on relative magnitudes of dielectric properties.

Early work in dielectric separation of minerals was reported by Hatfield in 1924 (1-2).[3] Experimentation with dielectric separation methods has been continued, up to recent times, by Debye (3), Pohl (4), Horgan (5), and Pickard (6). All these investigators used variations, in apparatus or applications, of Hatfield's original concept.

The Bureau of Mines, as part of its research to advance minerals technology, designed, tested, and patented a continuous dielectric separator in 1978 (7-8). This prototype laboratory-scale unit demonstrated efficiency for separating certain minerals from their associated gangue minerals. The unit generates a high-gradient, alternating electric field within a dielectric fluid medium. Mineral particles with dielectric constants higher than the dielectric constant of the fluid move in the direction of the highest field gradient, while mineral particles with dielectric constants lower than that of the fluid move in the direction of the lower field gradient. In the prototype dielectric separator (fig. 1), the highest electric field gradient surrounds small parallel wires on the surface of a cylindrical insulator called the drum electrode; the lowest electric field gradient occurs at the wire-screen electrode positioned 0.3 cm away from the drum-electrode wires. As shown in figure 2, a mineral mixture is fed onto the top of the rotating drum electrode and moves down between the two electrodes. High-dielectric minerals cluster around the small wires on the drum electrode. Low-dielectric minerals fall through the screen electrode to form the low-dielectric product. As the wires of the drum electrode rotate beyond the screen electrode, the high-dielectric minerals are released to form the high-dielectric product.

Throughout the many years of experimental work, a number of researchers have attempted to develop a fundamental understanding of dielectric separations (4-6, 9-10).

The dielectric force equation, developed from classical physics, has been applied successfully for interpretation of test results (10). Although many of these interpretations were only qualitative in nature, they provided some fundamental understanding of dielectric separations.
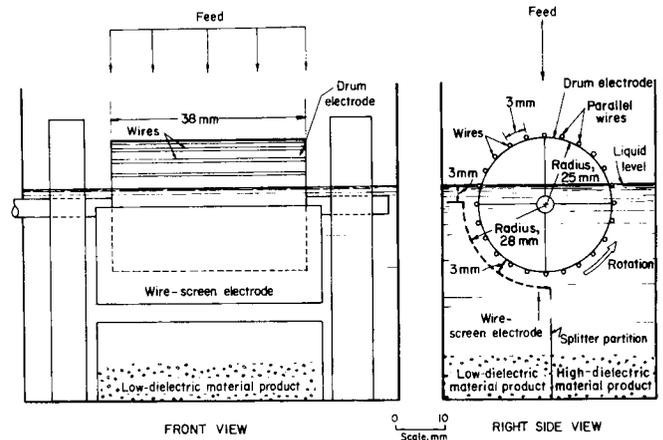
FIGURE 1.—Prototype dielectric separator for minerals.

KEY
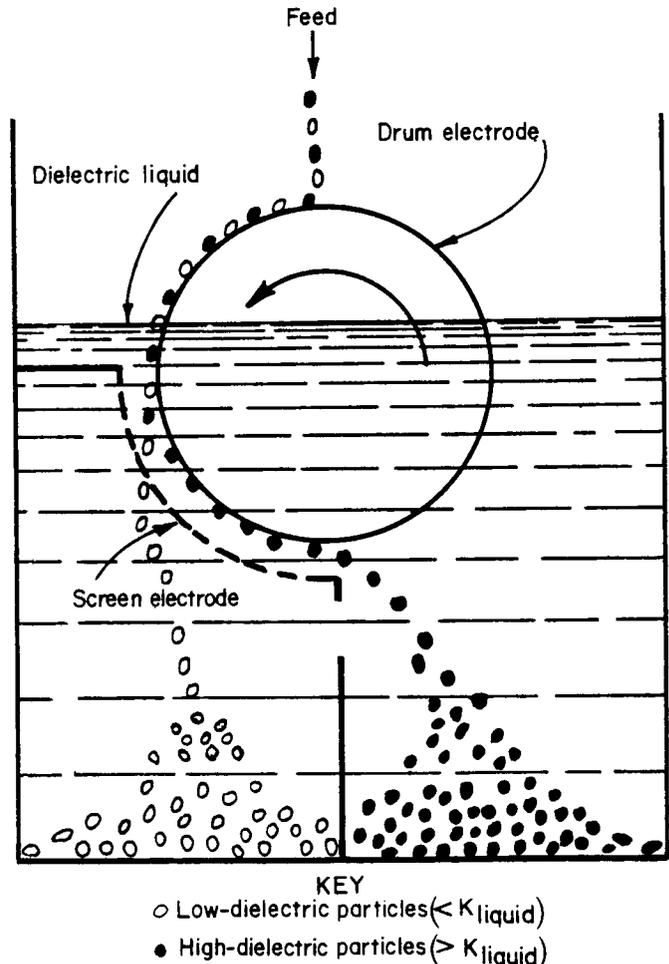o Low-dielectric particles($< K_{liquid}$)
● High-dielectric particles($> K_{liquid}$)

FIGURE 2.—Diagram of dielectric separation of minerals.

[3]Italic numbers in parentheses refer to items in the list of references at the end of this report.

The Bureau conducted the research described in this bulletin to provide a fundamental understanding of the design and operating characteristics of a dielectric separator. In addition to quantifying the dielectric force on the mineral particles, the factors opposing dielectric separation were also investigated. Gravity, inertia, diffusion, fluid drag, and current-induced polarization forces were studied along with the dielectric force to develop a comprehensive understanding of dielectric separation. The investigation was directed toward establishing limiting parameters for the electric field gradient, electrode geometry, voltage, electrical frequency, capacity, and liquid and mineral dielectric properties. The separator's dielectric force was derived from a theoretical interpretation of the electric field pattern and the dielectrical properties of the minerals and fluids. The significant opposing forces were calculated and compared with the dielectric force to predict separations of minerals. This report presents the experimental work and evaluation of both the empirical and theoretical studies to provide a fundamental understanding of dielectric minerals separation.

THEORY

Dielectric separation of mineral particles requires an appropriate balance of dielectric force with gravity, inertia, diffusion, fluid drag, and current-induced polarization forces. Each of these forces is calculated in the following sections.

DIELECTRIC FORCE

All solid matter consists of an assemblage of atoms, each composed of positive and negative charges, bound together by particular mechanisms. The characteristics of these bonding mechanisms determine the electronic properties of the material. In the case of metals, the metallic bonding mechanism consists of electric charges (the valence electrons) that are free to move throughout the material under the influence of an external electric field, providing electrical conductivity.

At the other extreme, ionically bonded insulators have no free charges to conduct electricity. All charges are associated with particular atoms and are known as bound charges. Most minerals fall somewhere between the extreme of cases of metals and insulators. In the presence of an external electric field, bound charges of opposite sign may be displaced from one another, giving the material a net electrical moment. It is this electric dipole moment, either permanent or induced, that gives a material dielectric properties. An electric dipole will orient itself along the electric field lines. The degree of polarization, or dipole moment per unit volume of the material, is represented by the dielectric constant or the dielectric permittivity.

Electric Dipole Force

An electric dipole consists of two equal and opposite charges, $+q$ and $-q$, separated by distance S. The electric dipole moment $\vec{p}$ is defined as $\vec{p} = q\vec{S}$. The force $\vec{F}$ exerted on a dipole of moment $\vec{p}$ by an electric field $\vec{E}$, considering the dipole to be two point charges separated by a distance S, is

$$\vec{F} = -q\vec{E} + q(\vec{E} + \vec{S} \cdot \nabla\vec{E} + \ldots), \tag{1}$$

$\nabla\vec{E}$ is the electric field gradient. In this equation, the field has been expanded about the point q, and only first-order terms are retained due to the fact that $\vec{S}$ is of the order of atomic dimensions. Then,

$$\vec{F} = -q\vec{E} + q\vec{E} + \vec{p} \cdot \nabla\vec{E} = \vec{p} \cdot \nabla\vec{E}. \tag{2}$$

The electric dipole moment induced in an isotropic particle is always in the direction of and proportional to $\vec{E}$. That is,

$\vec{p} = \alpha\vec{E}$, where α is a constant. Thus,

$$\vec{F} = \alpha\vec{E} \cdot \nabla\vec{E}, \tag{3}$$

where α contains the volume of the particle and the degree of polarization. It is clear from this equation that if the dielectric particle is in a uniform field (i.e., $\nabla\vec{E} = 0$), it experiences no electric dipole force. Increasing the electric field gradient proportionally increases the electic dipole force.

The force on a mineral particle immersed in a dielectric fluid can be developed from the classical interpretation of the simple dipole force equation developed above (equation 3). The net force due to the replacement of a dielectric fluid by a small dielectric sphere is equal to the product of the spherical volume, degree of polarization, electric field strength, and electric field gradient (4, 10). Several assumptions were made to obtain this relationship. A uniform electric field in an ideal dielectric fluid will be distorted by the insertion of a sphere of a different ideal dielectric. The degree of this distortion is given by

$$\text{polarizability factor} = 3\hat{\epsilon}_{fluid}\left(\frac{\hat{\epsilon}_{solid} - \hat{\epsilon}_{fluid}}{\hat{\epsilon}_{solid} + 2\hat{\epsilon}_{fluid}}\right), \tag{4}$$

where $\hat{\epsilon}_{fluid}$ and $\hat{\epsilon}_{solid}$ are the complex dielectric permittivities of the fluid and of the solid. This equation is based on the assumption that the electric field is nonuniform enough to produce an appreciable gradient across the particle and uniform enough to not sensibly alter the degree of polarization throughout the particle volume. If these equations are restricted to small spheres, the assumptions and the force equation (equation 3) are valid (4, 10).

The intensity of the local electric field $\vec{E}$ is equal to the negative gradient of the electric potential (voltage):

$$\vec{E} = -\frac{dV}{dS}, \tag{5}$$

where V is the voltage and dS is the differential distance.

Because $-\frac{dV}{dS}$ is a spatial derivative, the electric field is represented as the steepest downward slope (gradient) of the electric potential (voltage). The steepest downward slope is always normal to the equipotential surface and also represents the direction of the electric field vector.

The electric field gradient ($\nabla\vec{E}$) is the maximum upward slope of the electric field intensity:

$$\nabla\vec{E} = \frac{d\vec{E}}{dS} = \frac{d\left(-\frac{dV}{dS}\right)}{dS}. \tag{6}$$

This gradient can also be represented as the second derivative of the negative voltage gradient. The electric field intensity and electric field gradient are in the same direction. In an alternating current system with a sinusoidal voltage pattern, the direction of the electric field and electric field gradient vectors reverses each time the voltage sign changes from positive to negative. However, the product of these two vectors remains positive regardless of the voltage sign changes. Therefore, the voltage oscillations do not change the direction of the dielectric force vector.

Based on the previously developed equations, the dielectric force (F_e) equation can be written as

$$\vec{F}_e = \left(\frac{4}{3}\pi a^3\right)\left[3\hat{\epsilon}_{fluid}\left(\frac{\hat{\epsilon}_{solid} - \hat{\epsilon}_{fluid}}{\hat{\epsilon}_{solid} - \hat{\epsilon}_{fluid}}\right)\right]\vec{E} \cdot \nabla\vec{E}, \quad (7)$$

| particle volume | polarizability | electric field | electric field gradient |

where a is the particle radius.

To effect a dielectric mineral separation, the dielectric force on the mineral to be separated must be significantly different than the dielectric forces on the other minerals. From the dielectric force equation, it can be seen that the $\hat{\epsilon}_{solid} - \hat{\epsilon}_{fluid}$ portion of the polarizability factor can be manipulated by selecting the appropriate dielectric fluid. For example, a mixture of two minerals (A and B) with different dielectric permittivities, $\hat{\epsilon}_A$ and $\hat{\epsilon}_B$, where $\hat{\epsilon}_A > \hat{\epsilon}_B$, can be dielectrically separated by selecting a dielectric fluid with a $\hat{\epsilon}_{fluid}$ such that $\hat{\epsilon}_A > \hat{\epsilon}_{fluid} > \hat{\epsilon}_B$. Then, the dielectric force on mineral B will be in the opposite direction of the dielectric force on mineral A. Mineral A will be moved by the dielectric force towards the higher intensity electric field, separating it from mineral B.

Polarizability Factor

The absolute electrical permittivity of any material can usually be represented as a complex number: $\hat{\epsilon} = \epsilon - i \cdot \sigma/\omega$, where ϵ is the real portion of the permittivity, σ/ω is the imaginary portion, and i is the imaginary unit vector; σ is the electrical conductivity of the material, and ω is the angular frequency of the voltage oscillations (4). For ideal dielectric materials, usually one of the following assumptions is made: (1) The conductivity is so small that it makes no significant contribution to the absolute permittivity. (2) the frequency is high enough to keep the imaginary portion low enough that it has no effect on the absolute permittivity. Consequently, for an ideal dielectric material, $\hat{\epsilon} = \epsilon$ and $\epsilon = K\epsilon o$, where K is the dielectric constant and ϵo is the permittivity of free space ($\epsilon o = 8.854 \times 10^{-12}CV^{-1}m^{-1}$. Making this substitution into the polarizability factor, the following equation is obtained:

$$\text{Polarizability factor} = 3K_{fluid}\left(\frac{K_{solid} - K_{fluid}}{K_{solid} + 2K_{fluid}}\right)\epsilon o. \quad (8)$$

In equation 7, the dielectric force is therefore a direct function of the dielectric constants of the mineral and fluid. Again, the selection of the fluid dielectric constant is important for separating two minerals. But in addition to manipulating the direction of the dielectric force, the selection of the dielectric fluid can also be used to maximize the dielectric force. Figure 3 shows the polarizability factor as a function of K_{fluid}/K_{solid}.
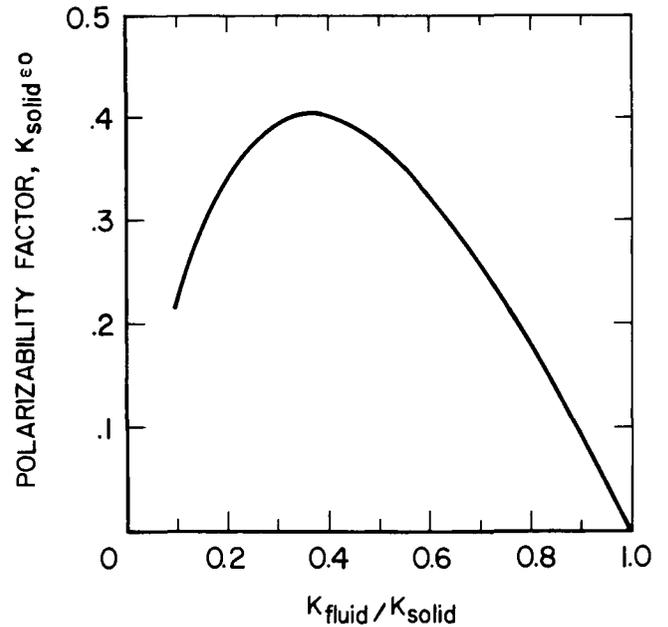
FIGURE 3.—Polarizability factor (see equation 8) versus K_{fluid}/K_{solid}.

The maximum polarizability factor for a mineral is obtained when the first derivative of the factor equals zero:

$$\frac{d\frac{\text{polarizability factor}}{K_{fluid}}}{} =$$
$$\frac{3K_{solid}^2 - 6K_{solid}K_{fluid} - 6K_{fluid}^2}{(K_{solid} + 2K_{fluid})^2}\epsilon o = 0 \quad (9)$$

The maximum polarizability factor is $0.402K_{solid}\epsilon o$ when the $K_{fluid} = 0.366K_{solid}$. The best dielectric fluid for recovering a dielectric mineral has (1) a dielectric constant lower than the dielectric constant of the mineral and higher than the dielectric constant of the gangue minerals and (2) has a fluid dielectric constant equal to 36.6 pct of the mineral's dielectric constant.

Voltage Configuration

In the dielectric force equation (equation 7) the electric field and the electric field gradient depend upon the separator design and the voltage. As described earlier, the prototype separator design consists of small, parallel wires on a rotating insulator drum, comprising one electrode, and a curved screen electrode positioned 3 mm from the drum electrode. In effect, each small wire on the drum electrode becomes a focal point for the electric field from the opposing portion of the screen electrode.

Based on the method of images, the electrical potential caused by a single wire on the drum electrode is equal to the electric potential caused by two parallel, straight lines oppositely charged (11). One line is the wire; the second line is located beyond the screen electrode such that the screen electrode is located midway between the two lines. For this configuration,

$$V = \frac{\Lambda}{2\pi\epsilon}\ln\frac{r_2}{r_1}, \quad (10)$$

where Λ = linear charge density on the two lines,

ϵ = permittivity of material between the lines,

r_1 = distance from the real line in the wire, and

r_2 = distance to the image line beyond the screen electrode.

From this equation it can be seen that the voltage is zero midway between the two lines, giving the screen electrode a uniform voltage and a uniform charge distribution. Each of the wires on the drum electrode can be represented this way. As shown in figure 4, the equal-potential lines for each pair of charged lines overlap several of the adjacent pairs. The total potential at any point between the drum and screen electrode is the sum of all the pairs of lines. The spacing between each wire and its image line was varied to satisfy the following conditions: First, the total voltage at each wire was equal, and second, the total voltage along the screen electrode was zero. The voltage at a point between the two electrodes then becomes

$$V_{total} = \frac{\Lambda}{2\pi\epsilon} \sum_{i=1}^{n} \ln \frac{r_{2_i}}{r_{1_i}}, \tag{11}$$

where n is the number of drum-electrode wires opposing the screen electrode.

Using polar coordinates with the origin at the rotational center of the drum electrode, figure 5 shows the trigonometry for the general voltage equation at point (r, θ). (The symbols r, θ, and others used in the rest of this paragraph are identified below equation 12.) Let $\delta_i = \Theta + (i - 1) \dfrac{S_w}{R + r_w}$, the angle between the radial to the ith wire pair and the radial to the particle at (r, Θ). For each real and image wire $r_{1_i}^2 = r^2\sin^2\delta_i + (r\cos\delta_i - R - r_w)^2$ and $r_{2_i}^2 = \sin^2\delta_i + (R + r_w + S_{m_i} - r\cos\delta_i)^2$. By taking the summation of all the wire pairs, the total voltage at point (r, Θ) is obtained:

$$V_{(r, \Theta)} = \frac{\Lambda}{2\pi\epsilon} \sum_{i=1}^{n} \ln \sqrt{\frac{r^2\sin^2\delta_i + (R + r_w + S_{m_i} - r\cos\delta_i)^2}{r^2\sin^2\delta_i + (r\cos\delta_i - R - r_w)^2}} \tag{12}$$

where $\delta_i = \Theta + (i - 1) \dfrac{S_w}{R + r_w}$.

The symbols used in these equations are identified as follows:

r = radial distance from center of rotation,

Θ = rotation angle of drum electrode

δ_i = angle from drum-electrode wire to particle location

S_w = spacing between wires on drum electrode,

R = radius of drum electrode,

r_w = radius of the wire on the drum electrode,

and S_{m_i} = spacing between each wire and its image wire.

By substituting $V = 0$ at $r = R + S_E + r_w$ (the position of the screen electrode), where S_E is the spacing between the electrodes, and $V = V_{max}$ at the surface of each of the wire electrodes, the $\dfrac{\Lambda}{2\pi\epsilon}$ constant and the S_{m_i} of each wire can be determined for each separator design. To solve these equations, a computer program was developed to make incremental adjustments in each S_{m_i} and then calculate the sum of the error squared for the solution. Using this method, the computer continued to make adjustments until the standard deviation error was less than 5 pct. At that point, the $\dfrac{\Lambda}{2\pi\epsilon}$ constant and the S_{m_i} of each wire then incorporated
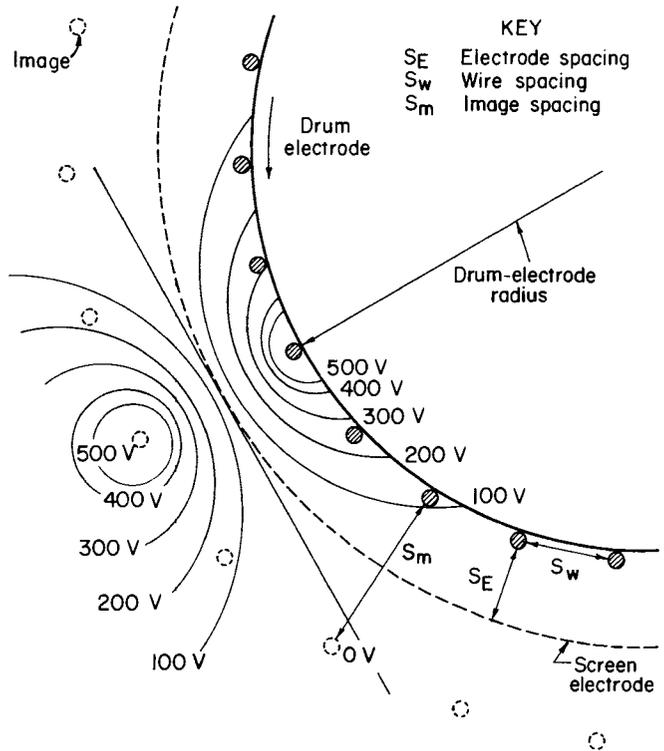
FIGURE 4.—Cross-sectional view of the dielectric separator showing configuration of drum-electrode wires, screen electrode, and image wires. Equal-potential lines are shown for one wire and image wire pair.
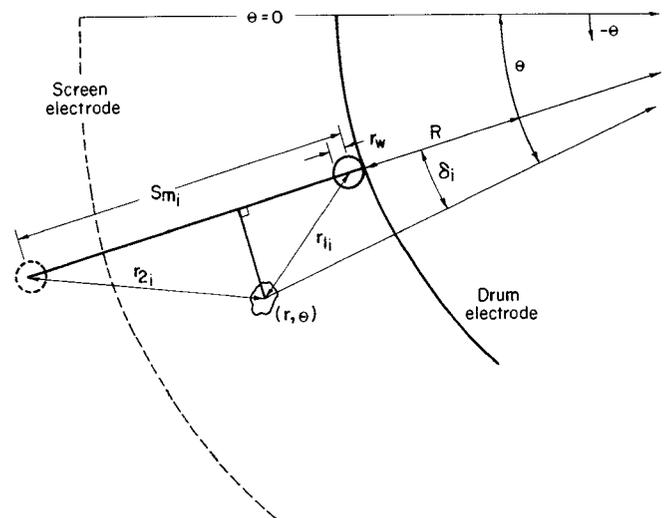
FIGURE 5.—Trigonometric relationship of particle at (r, Θ) and each drum-electrode wire. (See text, below equation 12, for identification of symbols.)

in the general voltage equation 12 for the particular separator design. Figure 6 shows the equal-potential lines between the electrodes for a 5-cm-diam dielectric separator with 1,000 V between the electrodes. The electrode spacing (S_E) was 0.32 cm, the wire spacing (S_w) was 0.32 cm, and the wire radius (r_w) was 0.027 cm. Figure 6 also shows the electric flux lines, which represent the direction of the electric field and the electric field gradient. These lines are always perpendicular to the equal-potential lines. They converge towards the wire electrodes, producing a high electric field gradient,

FIGURE 7.—Diagram of particle and electric field pattern for dielectric force calculation. (a = particle radius.)

FIGURE 6.—Equal-potential lines of the dielectric separator with 1,000 V across the electrodes. Electric flux lines converge towards each drum-electrode wire.

and are uniformly distributed at the screen electrode, where they produce no field gradient.

Using the general voltage equation for the 5-cm-diam separator design, the electric field was calculated by the following method: For a point (r, Θ), the orientation of the equal-potential line was determined by searching the area a very small distance (10^{-7} cm) from that point. Figure 7 should help to explain this technique. From the equal-potential line, the direction of the electric field (perpendicular) was determined. The voltages along that perpendicular line were calculated for a small distance (10^{-7} cm) from point (r, Θ). The difference between these voltages divided by twice that small distance equals the magnitude of the electric field. The electric field gradient was calculated by superimposing a small spherical particle with its center at the point (r, Θ). Along the same directional line of the electric field, the magnitude of the electric field at both sides of the particle was calculated. The electric field gradient across the particle equals the difference in these electric field magnitudes divided by the particle diameter. By incorporating the dielectric properties of the particle and the surrounding fluid media, the d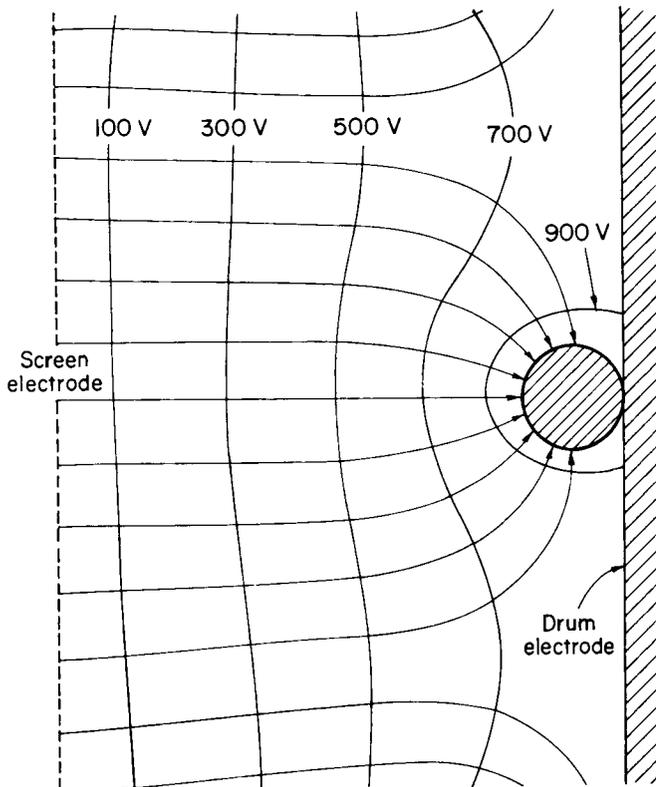ielectric force on the particle at point (r, Θ) was calculated. Again, utilizing the microcomputer, dielectric force maps for several particles sizes were calculated for the prototype dielectric separator design. Figure 8 shows the force map for a 100-mesh-size particle in the prototype dielectric separator. For this map the following conditions were used: 1,000 V across the electrodes, 0.32 cm wire-to-wire and electrode spacing, and 0.053 cm wire diameter. The dielectric force decreased sharply as the distance from the wire electrode increased. The direction of the dielectric force followed the same pattern as the electric field flux lines shown in figure 6.
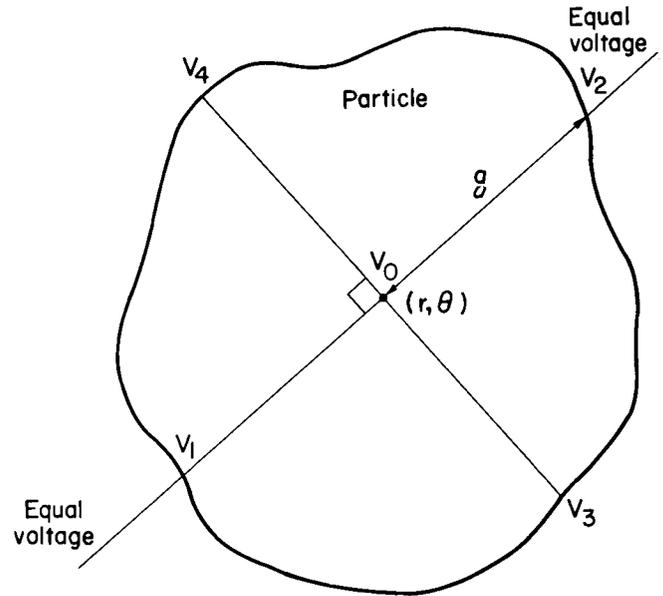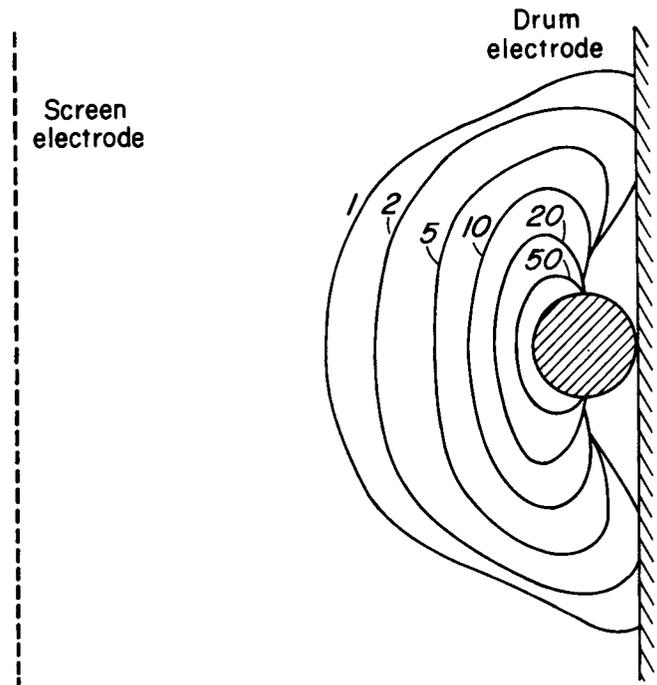
FIGURE 8.—Map of dielectric force (in millidynes—italic numbers) at 1,000 V for the drum-electrode wires.

OTHER FORCES

Before discussing the types and magnitudes of the opposing forces in the prototype dielectric separator, the path of a high-dielectric particle should be traced as it moves through the separator. Referring back to figure 2, the high-dielectric particle is fed onto the top of the rotating drum electrode. It remains on that surface until the drum rotation moves it into the dielectric fluid. As the particle moves between the two electrode, it is attracted to the wire on the

drum electrodes. It remains attached to the wire electrode until the drum rotates beyond the screen electrode. At that point the particle leaves the drum-electrode wires, settling through the fluid to join the high-dielectric product. The high-dielectric particle spends most of its time attached to the wire electrodes. Only forces opposing this particle attachment compete with the dielectric force. Among these forces are gravity, inertia, diffusion, fluid drag, and current-produced polarization forces. A diagram of these forces on a high-dielectric particle is shown in figure 9. To provide a better understanding of the separation of minerals with the prototype dielectric separator, each force is discussed individually below before the forces are combined into a single equation.

Gravity

Gravity (F_g) in the fluid is one of the major forces opposing the dielectric force:

$$F_g = (\varrho_s - \varrho_f) \, 4/3 \cdot \pi a^3 g, \tag{13}$$

where ϱ_s = density of the solid particle,
  ϱ_f = fluid density,
  g = acceleration of gravity (980 cm/s^2),
and a = particle radius.

The difference between the solid and fluid densities is used to correct for the buoyancy effect of the fluid. At the point of entry between the two electrodes, the gravitational force acts perpendicular to the dielectric force. However, as the drum rotates further between the electrodes, the radial component of gravity increases and reaches a maximum at the bottom of the drum-electrode rotation. At this point gravity acts directly against the dielectric force on a high-dielectric particle.

FIGURE 9.—Force diagram of a high-dielectric particle attached to drum-electrode wires.

Inertia

After a particle attaches to the drum electrode, its motion relative to the drum electrode is stationary. However, the rotation of the drum electrode produces an inertial or centrifugal force (F_i) upon the particle:

$$F_i = (\varrho_s - \varrho_f) \, 4/3 \cdot \pi a^3 \frac{4\pi^2}{3,600} r(D)^2, \tag{14}$$

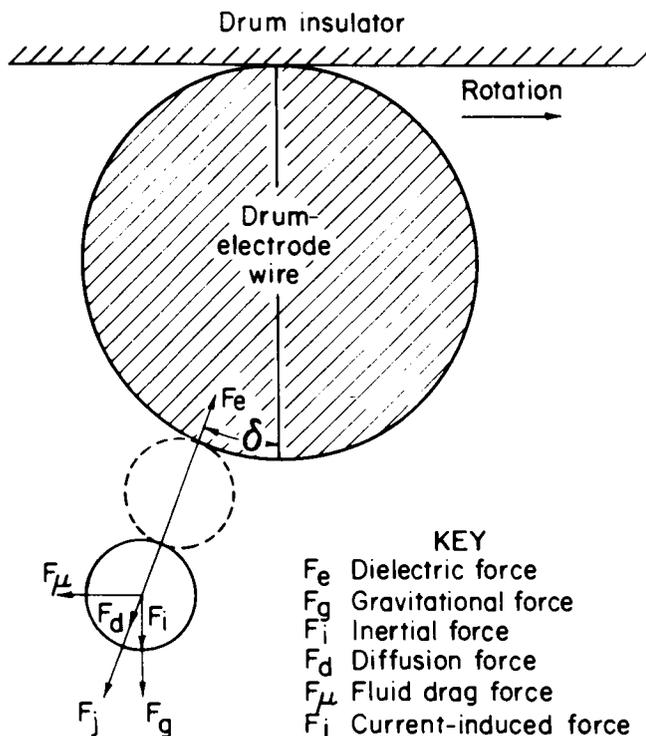where r is the radial distance from the rotating center of the drum electrode to the particle and D is the rotation speed of the drum electrode. The inertial force is always in the positive radial direction.

Diffusion

The Brownian-type diffusion force on the particles (F_d) is related to the concentration of particles in the fluid. This force tends to disperse the particles evenly throughout the fluid. As the particles enter the fluid, they are packed together on the surface of the drum electrode.

$$F_d = -BT \left(\frac{\Delta N}{N}\right)\left(\frac{1}{\Delta s}\right) \tag{15}$$

where B = the Boltzmann constant (1.38×10^{-16} erg/°),
  T = absolute temperature,
  $\dfrac{\Delta N}{N}$ = fractional change in particle concentration in the radial direction,
and Δs = change in radial direction corresponding to change in concentration.

The diffusion force is in the direction of lowest particle concentration. The maximum relative change in particle concentration $\left(\dfrac{\Delta N}{N}\right)$ over the smallest distance (Δs) corresponds to an empty area only one particle diameter away from the particle. Thus, if a is the particle radius, the maximum diffusion force is $F_d = \dfrac{-BT}{2a}$.

Fluid Drag

As the high-dielectric particle moves through the fluid to attach to the wires of the drum electrode, a viscous drag force (F_μ) acts against its motion. $F_\mu = -6 \, \pi a \mu S_p$, where μ is the viscosity, a is the particle radius, and S_p is the relative speed of the particle through the fluid. This drag force always acts against the motion relative to the fluid. Even after the particle attaches to the drum-electrode wires, the rotation of the drum electrode produces a relative fluid drag upon the particle. The rotation of the drum electrode causes the fluid between the two electrodes to flow in the same direction. Under laminar flow conditions, the velocity profile between the two electrodes is parabolic. This means that the velocity of the fluid is $S_f = \dfrac{2\pi D}{60} R \left(1 - \dfrac{(r-R)^2}{S_E^2}\right)$, where D is the rotation speed of the drum electrode, R is the radius of the drum electrode, r is the radial distance from the center of rotation, and S_E is the electrode spacing. The direction of the flow is tangential to the radial vector and in the same direction as the rotation. At the surface of the drum electrode, the fluid velocity (S_f) is the same as the peripheral speed of the drum electrode. At the screen electrode, the fluid velocity is zero. A particle attached to the wire on the drum

electrode will actually be moving faster than the fluid surrounding it. The particle velocity (S_p), relative to the fluid, is

$$S_p = \frac{2\pi D}{60}(R+a) - \frac{2\pi D}{60} R\left(1 - \frac{a^2}{S_E{}^2}R\right) \quad (16)$$

$$= \frac{2\pi D}{60}\left(a + \frac{a^2 R}{S_E{}^2}\right).$$

In the presence of several other attached high-dielectric particles, the particle could be attached farther away from the wire electrodes and subject to even higher fluid drag. The general equation for the fluid drag on an attached particle now becomes.

$$F_\mu = -6\pi a\mu\left(\frac{2\pi D}{60}\right)\left[r - R + \frac{(r-R)^2}{S_E{}^2}R\right] \quad (17)$$

in the tangential direction.

Current-Induced Polarization

The last opposing force to dielectric separation is caused by current-induced polarization. When the static-electrical conductivity of the fluid is greater than that of the particle, charges arriving at the surface of the particle are not conducted through the particle as fast as they are through the fluid. A net charge begins to develop on the particle surface, polarizing the particle along the lines of the current flow. This polarity is opposite to the dielectric polarity. In relatively static electric fields, the net charge on the particle surface continues to accumulate with time. Eventually, this current-induced polarization will effectively neutralize the dielectric polarization. Pohl (4) presents a force equation for current-induced polarization (F_j) in a slightly nonuniform electric field:

$$\vec{F}_j = (4/3 \cdot \pi a^3)\left[\frac{-3t(K_p\sigma_f - K_f\sigma_p)}{(K_p + 2K_f)}\right]\vec{E} \cdot \nabla\vec{E}, \quad (18)$$

| particle volume | polarizability | electric field | electric field gradient |

where t is time and σ_f and σ_p are the static-electrical conductivities of the fluid and particle, respectively. This equation is similar to the dielectric force equation (equation 7) except for the polarizability factor.

The importance of the current-induced polarization force on the prototype dielectric separation largely depends upon the amount of time the particle has to accumulate the current-induced polarization. For a 5-cm-diam dielectric separator turning at 15 r/min, a high-dielectric particle attached to a wire on the drum electrode is between the two electrodes for 1 s. In a static electric field, this is plenty of time for the particle, which has a relatively low conductivity, to accumulate enough charge to neutralize the dielectric polarity and be repulsed from the wire electrode. However, in an alternating electric field, the polarity on the particle reverses once each cycle. Consequently, the net charge accumulated by the surface of the particle during the first half of the electrical cycle is available to flow back into the fluid during the second half of the cycle. This means the maximum time for the particle to accumulate charge is half the cycle time. The current-induced polarization force increases during the first quarter of the cycle and decreases during the second quarter.

Although the polarity of the electrodes changes during the second half of the cycle, the direction of the current-induced polarization force remains the same. It always acts away from the high electric field regions.

At low electrical frequencies, the current-induced polarization may have enough time (half a cycle) to overcome the dielectric polarization. However, as the frequency increases, the current-induced polarization has less and less effect upon the dielectric polarization. For dielectric separations, the current-induced polarization of the high-dielectric particle should be minimized. This can be accomplished by two methods. A dielectric fluid can be selected with a static conductivity lower than that of the high-dielectric particle. This will prevent the accumulation of charge on the surface of the particle. The second method utilizes high electric frequencies to prevent current-induced polarization by shortening the formation time. Current-induced polarization is important only in a fairly static electric field, and can be ignored at electrical frequencies $\approx\ > 100$ Hz.

COMBINED FORCES

Most of the forces on a high-dielectric particle directly oppose the dielectric force. To keep a particle attached to the drum-electrode wire, the dielectric force must dominate the other forces throughout the pass between the two electrodes. The highest opposition to the dielectric force occurs when the drum-electrode wire is at the bottom of the drum rotation ($\Theta = 90°$). By vector addition (fig. 9), the minimum dielectric force to keep the particle attached is

$$\vec{F}_{e_{min}} = \vec{F}_j + \vec{F}_d + \sqrt{(\vec{F}_g + \vec{F}_j)^2 + (\vec{F}_\mu)^2}. \quad (19)$$

By calculating the forces shown in this equation, the effectiveness of the prototype dielectric separator can be predicted.

For example, the calculated forces on a particle in a typical dielectric separation of rutile from quartz are shown in table 1. In this example, a 5-cm-diam separator was used with 1,000 V across the electrodes and a 15-r/min rotation speed. The particle was assumed to be stationary relative to the drum electrode and 1.5 particle diameters from the drum-electrode wire, in a configuration similar to that shown in figure 9. So maximize the forces opposing attachment, the wire electrode was assumed to be at the bottom of the drum rotation. For these calculations, both rutile and quartz were assumed to be ideal dielectric materials so that their electrical permittivities were equal to their dielectric constants. At low frequency (10 Hz), a rutile particle was dominated by the current-induced polarity force pushing the particle away from the drum electrode (table 1). At high frequency (10,000 Hz), the rutile particle was held firmly to the drum-electrode wire by the dielectric force. The centrifugal force at 15 r/min was less than 1 pct of gravity and had little effect on the rutile particle. The diffusion force due to the concentration of particles around the wire was insignificant; this force can be ignored in most situations. The drum rotation appeared to produce significant viscous drag forces upon the particles. Fluid drag on a 210-μm-diam rutile particle was only 7 pct of gravity, but for a 75-μm-diam particle, the fluid drag on the rutile particle was almost half of gravity. Because this force is tangential, the attachment point of the particle is shifted by the fluid drag until the tangential component of the dielectric force counters the viscous drag force. This points out that

TABLE 1.—Typical forces for dielectric separation of rutile from quartz,[1] calculated values

(+ = towards drum electrode; − = away from drum electrode)

Forces on the particle 10⁻³ dyn	Rutile				Quartz			
	75 μm diam		210 μm diam		75 μ diam		210 μm diam	
	10 Hz	10 kHz	10 Hz	10 kHz	10 Hz	10 kHz	10 Hz	10 kHz
F_e	9.7	9.7	120	120	− 1.2	− 1.2	− 25	− 15
F_g	− .59	− .59	− 13	− 13	− .25	− .25	− 5.5	− 5.5
F_i	− .004	− .004	− .085	− .085	− .002	− .022	− .036	− .036
F_d	− 6 × 10⁻⁹	− 6 × 10⁻⁹	− 2 × 10⁻⁹	− 2 × 10⁻⁹	− 6 × 10⁻⁹	− 6 × 10⁻⁹	− 2 × 10⁻⁹	− 2 × 10⁻⁹
F_μ	− .35	− .35	− 1.46	− 1.46	− .35	− .35	− 1.46	− 1.46
F_j	− 97	− .10	− 1200	− 1.2	28	.03	350	.35
Total	− 88	8.9	− 1090	106	26.4	− 1.6	329	− 20

[1] Rutile: K = 115, σ_s = 1 × 10⁻¹³ mho/cm, ϱ = 4.2 g/cm³ (9, 29).
Fluid: K = 6, σ_s = 1 × 10⁻⁸ mho/cm, ϱ = 1.49 g/cm³, μ = 0.03 P (16).
Quartz: K = 4.3, σ_s = 1 × 10⁻¹⁵ mho/cm, ϱ = 2.65 g/cm³ (3, 28), for particle position as shown in figure 9.
Conditions: 5-cm-diam separator at 15-r/min drum rotation speed; 1,000 V across the electrodes. Dielectric fluid: acetone and perchloroethylene mixture.
[2] Acts tangentially to the drum electrode.

in addition to the magnitude of the dielectric force, the direction is also important. referring again to figure 9, if the dielectric force exactly balances the opposing forces of the high-dielectric particle, the particles to the left of this particle and surrounding the drum-electrode wire will have sufficient dielectric force in the tangential direction to keep them attached. However, particles to the right will be swept away from the drum-electrode wire by the fluid drag, because the tangential component of their dielectric force is in the wrong direction. In terms of the volume immediately surrounding the drum-electrode wire, the tangential dielectric force is only effective on the leeward side of the drum-electrode wire.

The quartz particle had dielectric, gravity, inertia, diffusion, and fluid drag forces all acting in directions away from the drum electrode. Only the current-induced polarization force attracted the particle toward the drum-electrode wire. At low frequency (10 Hz), the current-induced polarization force was much higher than the other forces, and the quartz particle remained attached to the drum electrode. However, at high frequency, the current-induced polarization force was much smaller, and the quartz particle fell from the drum electrode. As the quartz particle left the vicinity of the drum-electrode wires, the magnitude of the electric field and electric field gradient decreased rapidly. Soon, the particle was only free falling through the moving fluid. Only the gravity and fluid drag forces contributed to the particle's motion. As it first entered the space between the two electrodes, the quartz particle and the fluid were moving in the same direction. The particle then began to move farther from the drum electrode and into the slower regions of the laminar fluid flow. Eventually, the particle reached its terminal settling velocity and settled through the screen electrode. The maximum distance a particle must settle to reach the screen electrode is the sum of the drum-electrode radius and the electrode spacing. A free-settling particle in a stationary fluid represents the maximum residence times (t_{max}) of a settling particle between the two electrodes:

$$t_{max} = \frac{(R + S_E)2\mu}{(980)(9)(\varrho - \varrho_f)a^2}. \qquad (20)$$

During this time, the fluid flow moves the particle toward the high-dielectric product. For a 5-cm-diam drum electrode rotating at 15 r/min, the average (root mean square) fluid velocity in the electrode gap is 1.8 cm/s. The residence time of the fluid becomes 1.4 s. For a 75-μm-diam quartz particle, the free-settling residence time is 0.3 s, indicating that the particle settles quickly through the screen electrode before the fluid can push it into the high-dielectric product. However,

for a 25-μm-diam quartz particle, the free-settling residence time is 2.7 s. This particle has plenty of time between the electrodes to be easily swept into the high-dielectric product by the fluid flow. Thus, the effectiveness of the dielectric separator is reduced for very small particles.

The preliminary calculated values shown in table 1 only predict the forces acting upon a lone particle. The volume surrounding the leeward side of the drum-electrode wire with at least the minimum required dielectric attachment force represents the potential capacity of the separator. This volume can be determined from the dielectric force map of the drum-electrode wire. It is called the effective dielectric force volume (EDFV) and is the maximum potential capacity of the separator, in terms of volume per unit of wire length. This region of effective dielectric force represents the maximum possible separator capacity, without taking into account the interaction effects between the closely packed particles.

Maximum potential capacity equals $\varrho_b L_w N_w D \dfrac{A_f}{2}$, where

ϱ_b is the bulk density of the high-dielectric mineral, L_w is the length of the electrode wires (width of the separator), N_w is the number of wires per revolution, D is the rotation speed, and $A_f/2$ is the leeward-side region with at least the minimum dielectric attachment force.

At least four types of particle interactions occur. First, high-dielectric particles interact to form "pearl chains" within the electric field as shown in figure 10. A high-dielectric particle distorts the electric field immediately surrounding it in the fluid, creating a nonuniform electric field. Another high-electric particle with a similar distorted electric field surrounding it is attracted toward the high regions of the first particle's electric field. Both particles exhibit a mutual attraction. The particles tend to cluster or line up along the electric flux lines. This effect is often observed in the prototype dielectric separations. Figure 11 is a cross-sectional view of the dielectric separator showing three of the drum-electrode wires and the opposing screen electrode. Without an electric field (no voltage), the rutile particles are randomly oriented. However, with 1,000 V (10,000 Hz) across the electrodes, the rutile particles migrate to the drum-electrode wires and form "pearl chains" along the lines of the electric field patterns (fig. 11). This effect extends the effective dielectric force region and increases the capacity of the separator.

The electric flux lines are concentrated within the "pearl chain" of particles, which enhances the dielectric polarization. However, in the region immediately adjacent to these "pearl chains," the electric flux lines are widely distributed, even
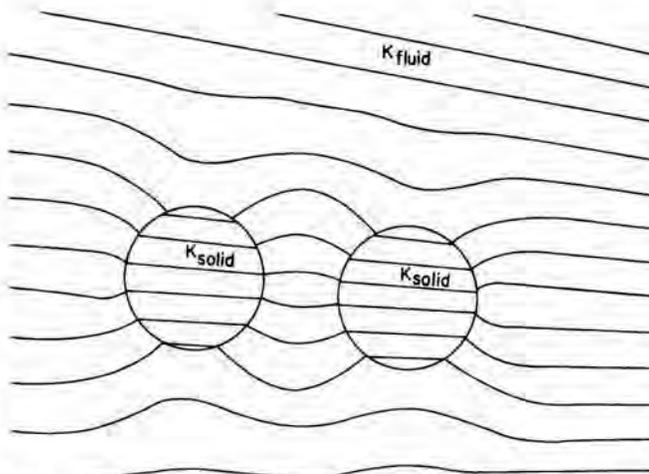
FIGURE 10.—Electric field distortion causing the "pearl-chain" effect between two high-dielectric particles.
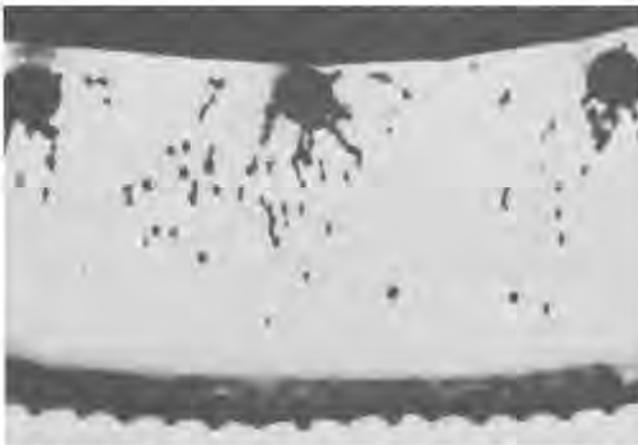

FIGURE 11.—Cross-sectional view of dielectric separator with rutile particles forming pearl chains along electric field lines.

more than they would be in the fluid without the high-dielectric particles present. In this adjacent region, the second interaction occurs. The wide distribution of the electric flux lines encourages low-dielectric material to reside in this region and reduces the effectiveness of high-dielectric particles recovery

The third type of interaction takes place between high-dielectric particles trying to attach to the drum-electrode wires and the low-dielectric particles leaving the drum-electrode surface. With a 10-wt-pct-rutile and 90-wt-pct-quartz mixture, there were 15 quartz particles for every rutile particle. Collisions between the particles result in much lower recovery of the high-dielectric particles. In general, to be attracted and remain attached, a high-dielectric particle must enter the electrode gap close enough to the drum electrode to pass into the EDFV surrounding the drum electrodes wires. The particle feed rate has a significant effect on recovery of the particle. The number of particle diameters from the drum-electrode wire to the minimum effective dielectric force region represents the maximum number of particle layers from which there will be good recovery of high-dielectric particles. High-dielectric particles in particle layers farther from the drum will probably not be recovered. Therefore, the maximum efficient capacity for the separator occurs at a particle layer feed rate equivalent to the number of particle diameters from the drum to the line of minimum effective dielectric force.

The fourth type of interaction takes place when the dielectric fluid is slightly more conductive than the low-dielectric mineral. When this condition exists, the current-induced polarity of the low-dielectric particles causes these particles to compete with the high-dielectric particles for the same regions of the high electric field intensity. This lowers both the recovery and grade of the high-dielectric product.

The magnitude of these particle interactions is difficult to predict. However, at feed rates below the maximum capacity, the effectiveness of the dielectric separator should be directly related to the EDFV. Variations in the separation parameters should show the corresponding variations in EDFV and in test results.

EXPERIMENTAL PROCEDURE

The theoretical calculations for dielectric separation were compared with experimental test results from a 5-cm-diam dielectric separator. A typical set of design and operating

TABLE 2.—Standard design and operating parameters for dielectric separation of rutile from quartz[1]

Design characteristics:
Drum electrode, cm:
Diameter 5.08
Wire diameter 0.053
Wire spacing 0.318
Wires per revolution 52
Screen-electrode screen size .... mesh.. 20
Electrode spacing .... cm.. 0.318
Separator width .... cm.. 3.8
Operating characteristics:
Drum-electrode rotation speed .... r/min.. 15
Voltage .... V.. 1,000
Electrical frequency .... Hz.. 10,000
Dielectric constant (K) of acetone-perchloroethylene mixture 6
Rutile in rutile-quartz mineral mixture .... pct.. 10
Feed rate (for 100-mesh particles) equivalent particle layers 1
Particle size range .... mesh.. −65, +200

[1] Parameter used in all tests except where individual parameters were investigated.

parameters was designated as "standard." These standard parameters (table 2) were used for every test except where individual parameters were investigated. A mixture of 10 pct rutile and 90 pct quartz was used, because both these minerals responded to dielectric separation. Only the minus 65- plus 200-mesh size range was used to minimize the effects of particle size. A screen analysis of the rutile and quartz mixture is shown in table 3. For convenience, the feed rate was based upon the equivalent monolayer of 100-mesh-size particles on the surface of the drum electrode.

Layers of particles were easily related to the EDFV to facilitate interpretation of the test results. For the rutile and quartz mixture, the 100-mesh particle layer was equivalent

TABLE 3.—Size analysis of minus 65- plus 200-mesh rutile and quartz mixture for standard tests

Size fraction, mesh	Wt pct	Rutile, pct	
		Analysis	Distribution
−65, +100	11	11.7	13
−100, +150	65	9.1	59
−150, +200	24	11.6	28
Composite	100	10	100

to 139 g/m² on the drum-electrode surface. At the standard operating condition of 15 r/min, the 5-cm-diam dielectric separator exposed 0.091 m² of surface area per minute. Therefore, 12.6 g/min was the standard for an equivalent 100-mesh particle layer feed rate. All other feed rates were considered to be a multiple or fraction of this 100-mesh particle-layer feed rate.

For each test, a small screw feeder was used to maintain a constant feed rate to the separator. A vibrating tray was used to evenly distribute the minerals on the drum electrode. Figure 12 shows the apparatus used with the 5-cm-diam dielectric separator. The actual width of the 5-cm-diam was 10.2 cm, but the vibrating tray was only 3.8 cm wide, so the effective separator width was only 3.8 cm, as shown in table 2. The fluid level in the separator was maintained about 0.5 cm above the screen electrode. The products from each test were collected in small glass trays beneath the separator. After each test, the products were filtered, dried, weighed, and analyzed. For each test product, rutile was separated from the quartz using heavy-liquid separation with acetylene tetrabromide. This technique was used to determine the rutile content of the test products; however, all other mineral separations were analyzed by accepted methods of chemical analysis.
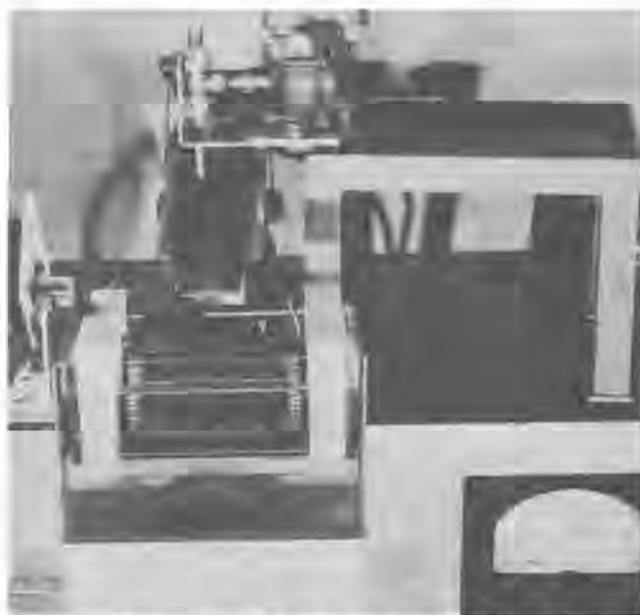

FIGURE 12.—Apparatus for dielectric separation of minerals.

EXPERIMENTAL RESULTS

RESULTS USING STANDARD PARAMETERS

Using the standard parameters, a 73-pct-rutile concentrate was produced, and 97 pct of the rutile was recovered. As shown in figure 13, this separation provided an immediate visual evaluation of the separator's performance. The maximum possible capacity (feed rate) without interparticle effects for the standard parameters was 25 g of rutile per minute, which corresponds to 250 g/min of the 10-pct-rutile mixture. This is equivalent to a feed rate of 20 particle layers. Figure 14 shows that the rutile recovery fell to 82 pct at 4 particle layers, to 41 pct at 12 particle layers, and to no separation with the separator hopelessly clogged at 20 particle layers. This indicated that interparticle effects significantly reduced the separator's effective capacity. The maximum particle-layer feed rate yielding at least a 95-pct-rutile recovery was three particle layers. This was predicted from the theoretical calculations that considered the distance from the drum-electrode wire to the region of minimum dielectric attachment force. For the standard condition, this distance was roughly three particle diameters. Because rutile was only 10 pct of the feed, particles in layers above the third particle layer (fourth, fifth, etc.) had a small probability of passing near enough to the drum-electrode wires to become attached. For efficient dielectric separation, the particle-layer feed rate should be equal to the number of particle layers of high-dielectric mineral that could attach to the drum electrode wires. By following this guideline, good recovery of the high-dielectric particles was maintained at a reasonably fast feed rate.

The theoretical equations did not predict quartz in the high-dielectric product. The EDFV for quartz at the standard conditions is zero. However, 27 pct of the high-dielectric product was quartz. This represented 4 pct of the quartz. As the rutile particles clustered around the drum-electrode wire, it is possible that some of the quartz particles might have become trapped by the rutile particles. Also, the fluid flow in the electrode gap could have swept a small portion of the

quartz particles into the high-dielectric product. Tests conducted with no voltage still recovered 2 pct of the quartz in the high-dielectric product. The grade of the high-dielectric product was not predictable from the theoretical calculations.

SEPARATOR DESIGN CHARACTERISTICS

Several design parameters affected the dielectric separation, including the wire spacing on the drum electrode, drum-electrode wire diameter, electrode spacing, screen-electrode mesh size, and drum-electrode diameter. The effects of each of these parameters were studied individually while holding all other parameters at the standard test conditions.

Drum-Electrode Wire Spacing

Using the standard operating condition, the rutile and quartz mixture was separated using drum-electrode wire spacings of 0.16, 0.32, and 0.64 cm. Figure 15 shows the experimental and calculated results. The rutile recovery ranged from 91 to 97 pct with the highest recovery at a wire spacing of 0.32 cm.

Over the same range of wire spacings, the EDFV showed a steady increase. The 0.16-cm wire spacing yielded four times as many wires as the 0.64-cm spacing. After adjusting EDFV according to the number of wires, the theoretical calculations did not show much difference between 0.32- and 0.64-cm wire spacing, but the EDFV for the 0.16-spacing was significantly lower. As the wire spacing decreased, the electric field became more uniform became and reduced the dielectric force on the particles. However, as the wire spacing increased, the number of wires decreased proprotionally, and the chance of a rutile particle entering the EDFV was also reduced, suggesting that a compromise might be necessary to obtain optimum separation results. This may help to explain why the rutile recovery was less than expected at the 0.64-cm wire spacing. The best wire spacing was 0.32

12

cm, because the EDFV was high and the rutile recovery was excellent.

Drum-Electrode Wire Diameter

Using the standard parameters, wires with three different diameters were tested on the drum electrode. The three diameters were 0.021, 0.053, and 0.080 cm. Figure 16

FIGURE 13.—The 5-cm-diam dielectric separator separating rutile from quartz.
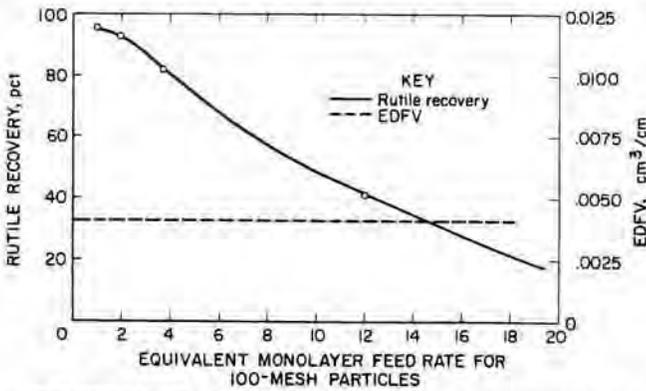

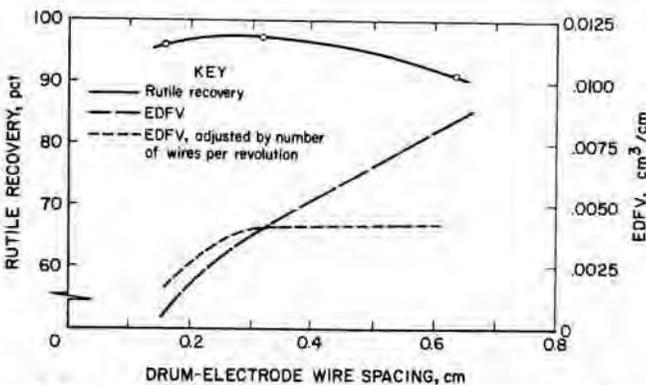FIGURE 14.—Equivalent particle layer feed rate versus rutile recovery.

FIGURE 15.—Effect of drum-electrode wire spacing on rutile recovery.

shows the experimental and theoretical results. Rutile recovery ranged from 92 to 97 pct, showing slightly better results when 0.053-cm-diam wire was used. It was expected that EDFV would decrease slightly with increasing wire diameter. However, both curves seem to indicate that the rutile recovery and EDFV were fairly consistent over the tested range of wire diameters. At each wire, the electric field converges toward a line within that wire. The volume of the large wire reduced the EDFV. However, this effect was not evident from the test results. At standard conditions, all three wire diameters had sufficient EDFV's to yield good rutile separation.

Electrode Spacing

Three spacings (0.16, 0.32, and 0.64 cm) between the drum and screen electrodes were tested, and the results are shown in figure 17. Rutile recovery decreased from a high of 98 pct using a 0.16-cm spacing to around 84 pct using a 0.64-cm spacing. The EDFV also decreased as the electrode spacing increased. The smallest electrode spacing (0.16 cm) was best. However, there are physical limitations on how close the electrodes can be positioned. The fabrication tolerances of the test separators precluded experimentation with closer electrode spacings.

Screen-Electrode Wire Mesh

Screen electrodes of five different mesh sizes were tested in the separator. The sizes were 10, 14, 20, 28, and 35 mesh. The results are shown in figure 18. The screen-electrode mesh size had virtually no effect on rutile recovery, and the
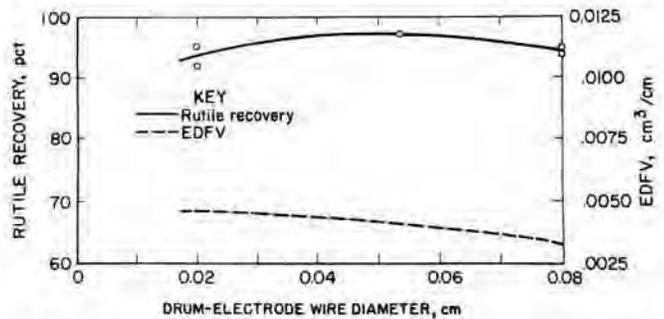

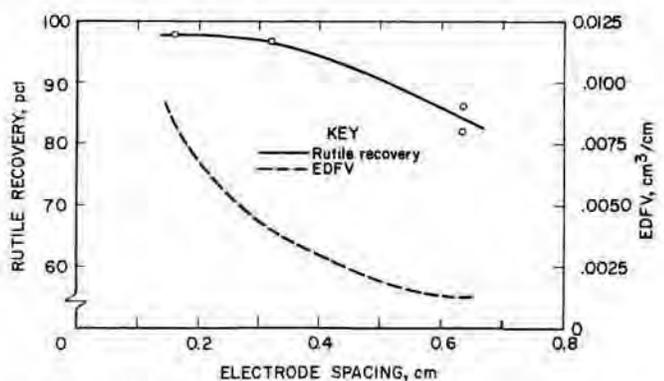FIGURE 16.—Effect of drum-electrode wire diameter on rutile recovery.

FIGURE 17.—Effect of electrode spacing on rutile recovery.

theoretical results predicted no effect on the EDFV. This finding and prediction confirmed the assumption that the screen electrode acts electrically like a solid electrode. The larger mesh screen electrodes were more desirable, because they offered the least resistance to settling of the low-dielectric particles.

Drum-Electrode Diameter

Separation with drum-electrode diameters of 2.5, 5.0, and 7.5 cm were tested at standard conditions. The results are shown in figure 19. Rutile recovery ranged from 84 to 97 pct. The best rutile recovery occurred using the 5-cm-diam drum electrode. The EDFV remained fairly constant, showing only a slight decrease as the drum-electrode diameter increased from 2.5 to 7.5 cm. As the diameter of the drum electrode increased, the peripheral speed of the drum's surface also increased proportionally, causing the fluid drag force on the particle to increase. For example, with the 2.5-cm-diam drum electrode, the fluid drag on a 100-mesh size particle was calculated as 0.0004 dyn; but for the 7.5-cm-diam drum electrode, the drag increased to 0.0012 dyn. These force calculations were based upon laminar flow characteristics in the electrode gap. With larger drum-electrode diameters, the flow pattern of the fluid between the electrodes would eventually become turbulent and reduce the EDFV.

Although a feed rate of only one particle layer was used for each drum-electrode-diameter test, the minerals feed rate were different. The 7.5-cm-diam drum electrode had three times more surface are per revolution than the 2.5-cm-diam drum electrode. Therefore, the 7.5-cm-diam separator treated
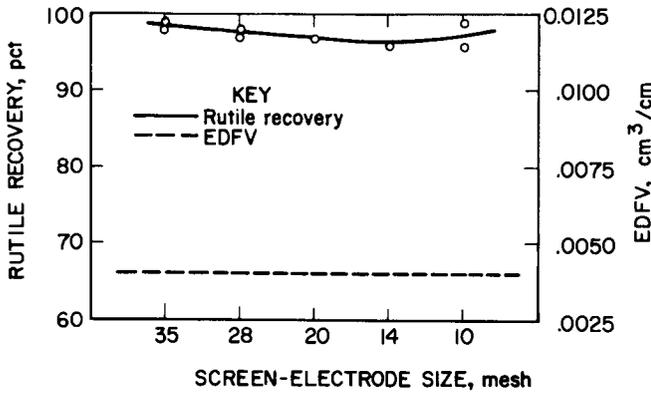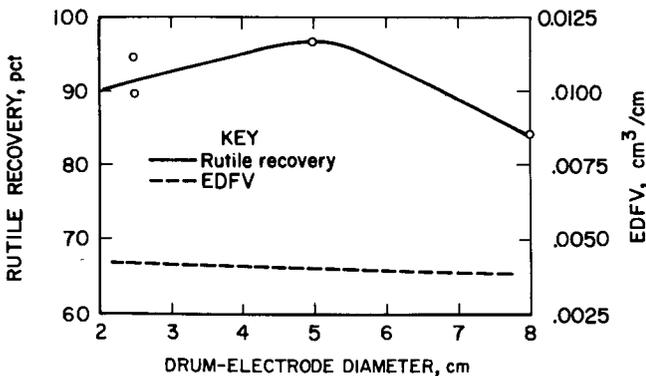
three times more material than the 2.5-cm-diam separator. From first appearances, the 7.5-cm-diam drum electrode recovered the rutile the fastest. However, as illustrated in figure 14, a 1.5-monolayer feed rate on the standard 5-cm-diam drum electrode recovered 96 pct of the rutile. This was better than the rutile recovery obtained at an equivalent feed rate on the 7.5-cm-diam drum electrode. In a statistical factorial design experiment using three rotation speeds, two dielectric fluids, and the three drum-electrode diameters, the 5-cm-diam gave significantly higher recoveries than those obtained using either the 2.5- or 7.5-cm-diam separator.

SEPARATOR OPERATING CHARACTERISTICS

Changes in the design characteristics had only small effects on the dielectric separations. A wider range of responses was obtained by varying the operating parameters, including electrode voltage, electrical frequency, drum rotation speed, particle size, dielectric constant of the fluid, and composition of the fluid.

Electrode Voltage

Using the standard test conditions (table 2), the electrode voltage was varied from 0 to 2,000 V. The resulting separations recovered from 0 to 98 pct of the rutile, as shown in figure 20. At 200 V and below, no rutile separation occurred. At 600 V, the rutile recovery was above 90 pct. Above 800 V, the rutile recovery showed very little change. The EDFV curve showed a near-linear increase for voltage above 600 V and predicted no rutile recovery at 200 V and below. The voltage of the electrodes was directly related to the energy consumption of the separator. To conserve energy, it was desirable to use the lowest effective voltage. The optimum voltage was 800 V, because 95 pct of the rutile was recovered while the voltage was kept fairly low.

Electrical Frequency

The electrical frequency was varied from 10 to 10,000 Hz. As shown in figure 21, rutile recovery was excellent at electrical frequencies above 500 Hz. At 10 Hz, the rutile recovery was only 60 pct. However, the EDFV calculation did not include the frequency factor. To simplify the force equations, the electrical frequency had been considered high enough to rule out the effects of (1) the dielectric conductivity of the minerals and the fluid and (2) the current-induced

FIGURE 18.—Effect of screen-electrode size on rutile recovery.

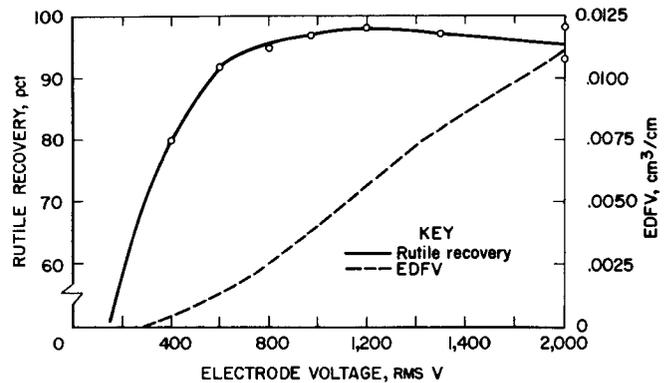FIGURE 19.—Effect of drum-electrode diameter on rutile recovery.

FIGURE 20.—Effect of electrode voltage on rutile recovery.

polarity effects of a fluid more conductive than the minerals Dielectric constant measurements at these frequencies (from a related but not yet published study by the authors) showed that the dielectric constant of the fluid remained fairly constant over the frequency range from 10 to 10,000 Hz. However, the dielectric conductivity factor (the imaginary portion of the electrical permittivity) of the fluid decreased from 1.6×10^{-9} to 9.3×10^{-12} over the same frequency range. This means that the absolute electrical permittivity of the fluid was much higher at 10 Hz than at 10,000 Hz. Similar measurements on rutile particles could not be obtained due to equipment limitations and the high-dielectric constant of the rutile. If the dielectric properties of rutile remain constant over the given frequency range, the polarizability factor of the dielectric force would be significantly lower at 10 Hz due to the increase in the dielectric conductivity of the fluid. This would result in a small EDFV and may be the reason for the low rutile recovery at 10 Hz.

As shown in table 1, the current-induced polarity is more significant at low frequencies. This polarity tends to neutralize the polarization of the rutile particles and reduce the EDFV. Consequently, the rutile recovery will drop. These negative effects can be effectively neutralized by using high electrical frequencies.

Drum-Electrode Rotation Speed

The rotation speed was varied from 5 to 30 r/min using the standard operating conditions. The results are shown in figure 22. At a one-particle-layer feed rate, the rutile recovery gradually declined from 99 to 91 pct as the drum speed increased. The EDFV also declined, showing good correlation with the rutile recovery curve. The actual feed rate to the separator depended upon both the drum speed and the
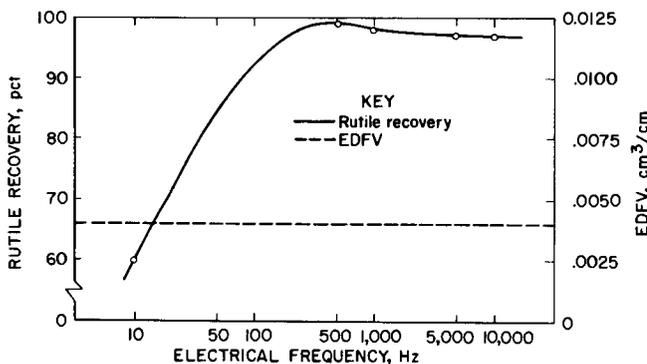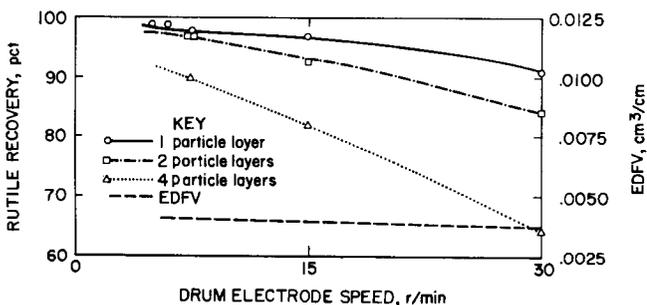
particle-layer feed rate. At the same actual feed rate, doubling the drum speed halved the particular-layer feed rate.

In figure 22, rutile recovery for the same actual feed rate remained fairly consistent. For example, at 7.5 r/min and four particle layers, the feed rate was 25 g/min with about 90-pct rutile recovery. At 30 r/min and one particle layer, the feed rate was still 25 g/min and the rutile recovery was likewise about 90 pct. However, the grade of the high-dielectric product was much lower at 30 r/min than it was at 7.5 r/min. Table 4 shows the rutile grade of the high-dielectric product at three rotation speeds and three actual feed rates. The best grade was obtained at the lowest drum-electrode speed.

TABLE 4.—High-dielectric product grade at various feed rates and drum-electrode speeds

Actual feed rate, g/min	Product grade, pct at—		
	7.5 r/min	15 r/min	30 r/min
12.6	91	73	ND
25.2	94	87	60
50.4	ND	91	43

ND Not determined.

Particle Size

A mixture of rutile and quartz ranging from 48 to 400 mesh size was tested at standard conditions. Table 5 shows the size analysis of this sample. The results for each size fraction are shown in figure 23. Rutile recovery increased gradually from 91 to 96 pct with decreasing particle size between 48 and 200 mesh, but dropped sharply at sizes smaller than 200 mesh. Likewise, the EDFV increased gradually with decreasing particle size between 48 and 200 mesh, and also decreased for particle sizes smaller than 200 mesh. This decreasing EDFV at sizes below 200 mesh, which can be traced to the fluid drag, showed good correlation with test

TABLE 5.—Size analysis of minus 48- plus 400-mesh mixture of rutile and quartz

Size fraction, mesh	Wt pct	Rutile, pct	
		Analysis	Distribution
−48, +65	6.3	10.2	6
−65, +100	6.9	11.8	8
−100, +150	40.6	9.2	37
−150, +200	15.0	11.6	17
−200, +270	18.7	6.4	12
−270, +400	12.5	16.0	20
Composite	100.0	10.1	100

FIGURE 21.—Effect of electrical frequency on rutile recovery.

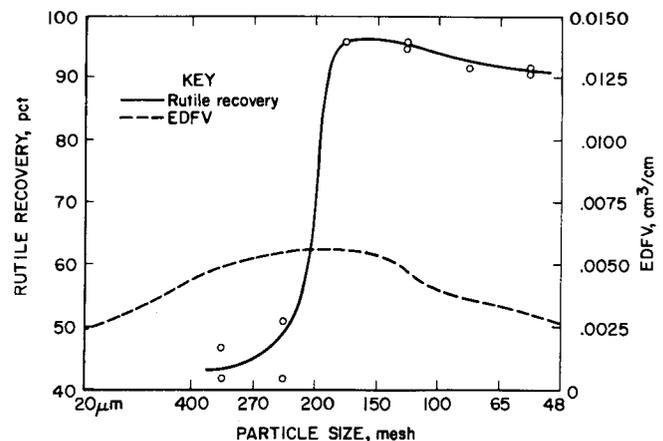FIGURE 22.—Effect of drum-electrode rotation speed on rutile recovery.

FIGURE 23.—Effect of particle size on rutile recovery.

results. Table 6 shows a summary of the forces acting on each particle.

From 20- to 150-mesh size, gravity was the dominant opposing force. At 200-mesh size, gravity and viscous fluid drag were about equal; below 200 mesh, the viscous drag was the dominant force. Both gravity and dielectric forces were proportional to the particle diameter cubed, but the viscous drag force was proportional to the particle diameter squared. Therefore, below 200-mesh size, the viscous drag force not only dominated the other opposing forces, but it overwhelmed the dielectric force, drastically reducing the EDFV. The viscous drag of the fluid is caused by the drum rotation. Reducing the drum-electrode rotation speed would shift the curves in figure 23 to the left; that is, recovery would be improved for the finer size fractions.

TABLE 6.—Forces acting on particles of different sizes during separation, millidynes

Particle size, mesh	F_g	F_i	F_μ	Minimum F_e
20	'800	5	7	− 805
35	'100	.6	2	− 101
48	'35	.2	1.5	− 36
65	'13	.08	1.2	− 13
100	'4.4	.028	.9	− 4.5
150	'1.6	.01	.7	− 1.7
200	.6	.004	.5	− .8
400	.07	.0005	'.23	− .24
740 (20 μm)	.01	.00007	'.094	− .094
1,480 (10 μm) ...	.001	.000009	'.043	− .043
2,960 (5 μm)	.0002	.000001	'.018	− .018

' Dominant opposing force.

Fluid Dielectric Constant

The dielectric fluid was usually a mixture of two pure miscible fluids. One fluid had a relatively low dielectric constant and the other had a relatively high dielectric constant. Mixing two such fluids in various proportions will yield dielectric fluids with dielectric constants anywhere between the dielectric constants of the two pure fluids. Ideally, the sum of the volume percent portion of each fluid times its dielectric constant was equal to the dielectric constant of the fluid mixture. This approximation,

$$K_{fluid} = V\%_A K_A + V\%_B K_B, \qquad (21)$$

was fairly accurate for most fluid mixtures.

Mixtures of acetone (K = 21.3) and perchloroethylene (K = 2.3) were tested from K = 4 to K = 21.3 (pure acetone). The results are shown in figure 24. The rutile recovery peaked at K = 6 and steadily fell as the fluid dielectric constant increased. Contrary to this trend, the EDFV gradually increased as the fluid dielectric increased. These opposing trends seemed to indicate that rutile and/or the fluid were not ideal dielectrics. Measurements of the dielectric properties of the fluid showed that the dielectric conductivity of the mixture increased rapidly as the dielectric constant increased.
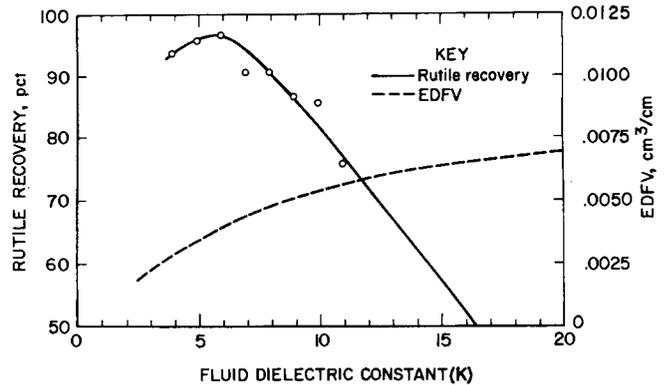

FIGURE 24.—Effect of the separator fluid's dielectric constant on rutile recovery.

Table 7 shows how the effective dielectric constant (equation 22) of the fluid mixture increased as the conductivity factor became more and more significant.

$$K_{effective} = \sqrt{K^2_{ideal} + \left(\frac{\sigma}{\omega \epsilon_0}\right)^2} \qquad (22)$$

TABLE 7.—Dielectric separation of rutile from quartz at different fluid dielectric constants

Tangent loss factor	Dielectric constant (K)			EDFV, cm³/cm	Rutile recovery, pct
	Real	Imaginary	Effective		
0.0464	4	0.186	4	0.0030	94
0.185	6	1.11	6.1	.0041	97
1.27	8	10.15	12.9	.0065	91
2.91	10	29.1	30.8	.0087	86
13.6'	15	204	205	0	10
124.8'	21.3	2658	2661	0	4

' Extrapolated from conductivity measurements of the fluid.

At K = 10, the effective dielectric constant of the fluid had risen to 30.8. With pure acetone, the effective dielectric constant was well above that of rutile (K = 115), indicating that rutile could not be recovered. This prediction correlated well with the rutile recovery obtained with a pure acetone dielectric fluid. As the dielectric conductivity rose, the energy consumption also increased. The dielectric constant of the optimal dielectric fluid should be high enough to efficiently separate the high-dielectric mineral while still keeping the fluid's dielectric conductivity low. For an acetone and perchloroethylene mixture, the best separation occurred at K = 6.

Dielectric Fluids

Fluids with the same dielectric constant may perform differently in a dielectric separator according to their dielectric conductivities. Five dielectric fluids were tested at standard conditions with an ideal dielectric constant of 6. The results are shown in table 8. Although the real portion of the

TABLE 8.—Dielectric separation of rutile from quartz using different fluids

	Ethanol-kerosene	Acetone-trichloro-ethylene	Acetone-perchloro-ethylene	Acetone-kerosene	Nitro-benzene-kerosene
Dielectric conductivity .....mho · m..	7.6 × 10⁻⁶	5.3 × 10⁻⁶	6.2 × 10⁻⁷	4.7 × 10⁻⁷	2.8 × 10⁻⁷
Effective dielectric constant (K)	37.3	21.0	6.2	6.1	6.0
EDFV ....cm³/cm..	0.0083	0.0079	0.0041	0.0033	0.0034
Density ....g/cm³..	0.85	1.30	1.49	.85	0.90
Viscosity ....cP..	0.017	0.025	0.030	0.015	0.0020
Rutile recovery ....pct..	92	92	97	92	85
Energy consumption (kW · h)/mt..	11.5	8.0	0.91	0.72	0.43

dielectric constant was 6, the effective dielectric constant (the vector sum of the real and imaginary portions) was different.

The dielectric fluid has a significant effect on the energy consumption of the dielectric separator. The average power (P_{av}) to the separator was $P_{av} = V^2/Z\cos\phi$, where V is the voltage, Z is the impedance of the separator, and $\cos\phi$ is the power factor. The inverse impedance was $(1/Z) = \sqrt{G^2 + \omega^2 C^2}$, where G is the conductance of the separator, ω is the angular velocity, and C is the capacitance of the separator. Substituting $G = \omega C\tan\delta$ (where $\tan\delta$ is the tangent loss factor) and $\phi = 90° - \delta$ in the inverse impedance equation, then

$$1/Z = \omega C\sqrt{(\tan\delta^2 + 1)} = \omega C\frac{1}{\cos\delta}; \qquad (23)$$

and therefore

$$P_{av} = V^2\omega C\frac{\cos\phi}{\cos\delta} = V^2\omega C\tan\delta. \qquad (24)$$

The 5-cm-diam separator had a measured capacitance of 13 pF/cm in terms of the drum-electrode length. With the K = 6 acetone and perchloroethylene dielectric fluid, the tangent loss factor was only 0.185. Therefore, the $P_{av} = (1,000)^2(2\pi10^4)(6 \times 13 \times 10^{-12})(0.185) = 0.88$ W/cm. At standard conditions, the energy consumption of the dielectric separator was 0.91 (kW · h)/mt. Energy consumption using several other fluids is shown in table 8.

The power consumed by the separator was a function of voltage, frequency, fluid dielectric constant, and the tangent loss factor. As the frequency dropped, the tangent loss increased. Figure 25 shows that energy consumption decreased as the frequency decreased. As shown in figure 21, rutile recovery was good at frequencies above 500 Hz. Therefore, the optimum energy consumption occurred at around 500 Hz. At this frequency, the energy consumption was lowered to 0.28 (kW · h)/mt.

MINERAL SEPARATIONS

Several different mineral mixtures were tested with the prototype separator to demonstrate its effectiveness. Table 9 shows the results of these separations. All of the tests were conducted at standard conditions, except for the fluid dielectric constant and the particle-layer feed rate. The dielectric constant of the fluid was selected to be near the dielectric constant of the low-dielectric mineral. The particle-layer feed rate was roughly inversely proportional to the high-dielectric mineral content of the feed mixture. These selected mineral separations showed the performance of the dielectric separator over a wide range of mineral mixtures.

The separation of rutile from quartz demonstrated that the separator is effective on minerals with a relatively large
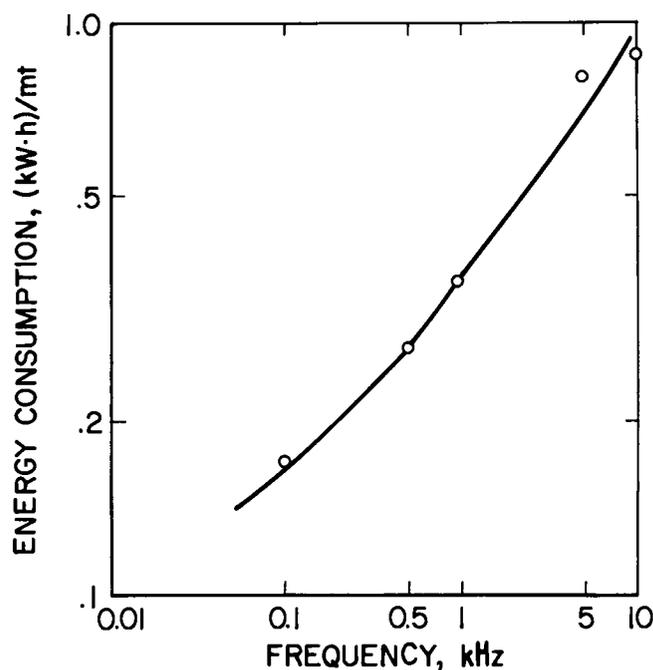

FIGURE 25.—Effect of electrical frequency on energy consumption.

difference in dielectric constants. The separation of zircon and collophane from quartz showed that the separator is effective on minerals with relatively low dielectric constants and with a substantial difference in dielectric constants. A 67-pct-zircon concentrate was obtained with 69-pct recovery of the zircon. The low EDFV may have been the reason for the low zircon recovery. A 91-pct-collophane concentrate was obtained with 85-pct recovery of the phosphate mineral. The higher concentration of collophane in the feed mixture necessitated the lower particle-layer feed rate (table 9).

The separation of collophane from calcite showed the effectiveness of the separator when there is a small difference in the minerals' dielectric constants. An 81-pct-collophane concentrate was produced with 90-pct recovery of the collophane. The dielectric constant of the fluid was only 7, which was smaller than that of both the collophane and the calcite. However, using the dielectric conductivity factor, the effective dielectric constant of the fluid was found to be 8.8, which lies between the dielectric constants of the two minerals.

Rutile was separated from zircon to demonstrate the effectiveness of the separator on minerals with dielectric constants above 10. The high-dielectric fluids are usually more conductive, which increases energy consumption during a separation. An 88-pct-rutile concentrate was obtained with 99-pct recovery of the rutile. Again, the dielectric constant

TABLE 9.—Mineral separation results

| Mineral mixture | | | | High dielectric | | | | | Particle | Energy |
| High dielectric | | Low dielectric | | Feed pct HD[1] | Conc., pct HD[1] | Recovery, pct | K_{fluid} | EDFV, cm³/cm | layer feed rate | consumption, (kW · h)/mt |
Mineral	K	Mineral	K							
Rutile	115.0	Quartz	4.3	10	73	97	6	0.0040	1	0.91
Zircon	11.8	..do........	4.3	10	67	69	6	.0009	1	.89
Collophane ...	9.2	..do........	4.3	32	91	85	5	.0014	.3	1.61
Do.	9.2	Calcite	8.3	44	81	90	7	.0014	.3	12.2
Rutile	115.0	Zircon	11.8	50	88	99	10	.0056	.2	42.4
Chromite	10.6	Olivine	7.8	30	50	88	8	.0004	.2	31.9
Chalcopyrite ..	>81	Quartz	4.3	1.1	59	93	7	.0045	1.9	1.8

[1] High-dielectric mineral.

of the fluid was lower than that of the zircon, but the effective dielectric constant was much higher than that of zircon.

Chromite could be separated from olivine, but the results were not good for a single pass through the separator. The EDFV for chromite was the lowest among these minerals, but this does not explain the low grade of the separation product. A large portion of the olivine was captured by the drum-electrode wires. Both chromite and olivine are minerals with relatively variable compositions, and this variation in composition may affect their dielectric properties, making separation difficult.

The separation of chalcopyrite from quartz demonstrated that the separator can effectively recover a high-grade concentrate from a low-grade feed. A 59-pct-chalcopyrite (20-pct-Cu) concentrate was obtained, recovering 93 pct of the copper.

CONCLUSIONS

Dielectric separation using the Bureau of Mines prototype dielectric separator has been demonstrated in the laboratory as an effective method for mineral separation. Fundamental equations of the dielectric force on the particles were derived to analyze performance of the prototype separator as a function of EDFV. The EDFV proved to be a qualitative prognosticator of separator effectiveness. Among the design characteristics investigated, the electrode spacing was the most sensitive for the recovery of the high-dielectric mineral. The other parameters had relatively minor effects on dielectric separations. Good separations were obtained with electrode spacings of less than 0.4 cm. At those spacings, the electric field convergence on the drum-electrode wires was sufficient to produce a high EDFV for the high-dielectric minerals.

All of the operating characteristics impacted significantly upon the effectiveness of the separator. The optimum range for each parameter is listed below, along with pertinent comments.

Electrode voltage: 800 V
1. High enough for efficient separation.
2. Low enough to minimize the energy consumption of the separator.

Electrical frequency: 500 Hz
1. High enough to overcome the effects of—
    a. The dielectric conductivity of the fluid and minerals.
    b. Current-induced polarization of the particles in a fluid more conductive than the mineral particles.
2. Low enough to minimize the energy consumption of the separator.

Drum rotation speed: 7.5 r/min (to minimize the fluid drag on the high-dielectric particles).

Feed rate: Three 100-mesh particle layers (for separating rutile from quartz)
1. High enough to fill the EDFV around each drum-electrode wire.
2. Low enough to allow each high-dielectric particle to pass within the EDFV.

Particle size: minus 48- plus 400-mesh
1. Small enough to allow the low-dielectric particles to settle freely through a 20-mesh screen electrode.
2. At a drum rotation speed of 7.5 r/min, using the 5-cm-diam separator, the fluid drag force was reduced, and the dielectric force was allowed to dominate.

Dielectric fluid: dielectric constant of 6 (for separating rutile from quartz)
1. High enough effective dielectric constant to prevent attraction of the low-dielectric mineral.
2. Low enough effective dielectric constant to maximize the EDFV for the high-dielectric mineral.
3. Low dielectric conductivity to minimize energy consumption.

Selected mineral separations demonstrated that—
1. Excellent separation was obtained from a mixture of high-dielectric minerals (K > 81) and low-dielectric minerals (K < 10).
2. Good separation was obtained from a mixture of minerals whose dielectric constants differed by approximately 2 or more.
3. Good separation was obtained from a mixture of two relatively high-dielectric minerals.
4. Good separation was obtained from a low-grade mineral mixture.

REFERENCES

1. Gaudin, A. M. Principles of Mineral Dressing. McGraw-Hill, 1939, pp. 467-470.

2. Hatfield, H. S. Dielectric Separation: A New Method for the Treatment of Ores. Bull. Inst. Min. & Met., v. 233, 1924, pp. 335-342.

3. Debye, P., and B. H. Eckstein. Dielectric High Frequency Method for Molecular Weight Determinations. Phys. Rev., v. 94, 1954, pp. 1412.

4. Pohl, H. A. Dielectrophoresis. Cambridge Univ. Press, 1978, 579 pp.

5. Horgan, H. D., and D. L. Edwards. Forces in Dielectric Fluids. J. Appl. Phys., v. 32, No. 9, 1961, p. 1784.

6. Pickard, W. F. The Interaction of Electrophoretic and Dielectrophoretic Forces. J. Electrochem. Soc., v. 111, No. 11, 1964, pp. 1234-1238.

7. Jordan, C. E., and C. P. Weaver. System for the Dielectrophoretic Separation of Particles and Granular Material. U.S. Pat. 4,100,068, July 11, 1978.

8. Jordan, C. E., G. V. Sullivan, B. E. Davis, and C. P. Weaver. A Continuous Dielectric Separator for Minerals Beneficiation. BuMines RI 8437, 1980, 18 pp.

9. O'Konski, C. T. Electric Properties of Macromolecules. Theory of Ionic Polarization in Polyelectrolytes. Univ. CA Press, 1960, pp. 605-619.

10. Von Hippel, A. R. Dielectrics and Waves. Wiley, 1954, 284 pp.

11. Boast, W. B. Principles of Electric and Magnetic Fields. Harper & Brothers, 1956, pp. 275-314.